Journal of Power Sources 255 (2014) 341–354

Contents lists available at ScienceDirect

Journal of Power Sources

journal homepage: www.elsevier.com/locate/jpowsour

# Optimized efficiency of all-electric ships by dc hybrid power systems

Bijan Zahedi [a,*], Lars E. Norum [a], Kristine B. Ludvigsen [b]

[a] Department of Electrical Power Engineering, Norwegian University of Science and Technology (NTNU), Trondheim 7491, Norway
[b] Research and Innovation, Maritime Transport, Det Norske Veritas (DNV), Hovik 1322, Norway

## HIGHLIGHTS

- Detailed efficiency analysis of a shipboard dc hybrid power system is carried out.
- An optimization algorithm is proposed to minimize fuel consumption under various loading conditions.
- An online optimization strategy for fuel saving is implemented in MATLAB/Simulink.
- An offshore support vessel (OSV) is simulated over different modes under online optimization control.
- The method achieves around 15% fuel saving with optimally utilized energy storage in the studied dc system.

## ARTICLE INFO

*Article history:*
Received 16 August 2013
Received in revised form
4 January 2014
Accepted 7 January 2014
Available online 15 January 2014

*Keywords:*
Efficiency optimization
Shipboard power system
dc distribution
Fuel saving
All-electric Ships

## ABSTRACT

Hybrid power systems with dc distribution are being considered for commercial marine vessels to comply with new stringent environmental regulations, and to achieve higher fuel economy. In this paper, detailed efficiency analysis of a shipboard dc hybrid power system is carried out. An optimization algorithm is proposed to minimize fuel consumption under various loading conditions. The studied system includes diesel engines, synchronous generator–rectifier units, a full-bridge bidirectional converter, and a Li-Ion battery bank as energy storage. In order to evaluate potential fuel saving provided by such a system, an online optimization strategy for fuel consumption is implemented. An Offshore Support Vessel (OSV) is simulated over different operating modes using the online control strategy. The resulted consumed fuel in the simulation is compared to that of a conventional ac power system, and also a dc power system without energy storage. The results show that while the dc system without energy storage provides noticeable fuel saving compared to the conventional ac system, optimal utilization of the energy storage in the dc system results in twice as much fuel saving.



## 1. Introduction

Increasing concerns on environmental issues and fuel economy have forced the maritime transport sector to pursue low emission and fuel efficient solutions. Power electronics plays a major role in optimization of the conventional drivetrains. In marine vessels, power electronic converters made a breakthrough with regard to fuel saving, when they enabled electrification of propulsion systems through Variable Speed Drives (VSDs) in 1990's [1]. The advantages gained from electric propulsion systems have ever since promoted the concept of all-electric ship, which provides a common electrical platform to supply the propulsion power and ship-service loads [1–3]. Although the overwhelming majority of present all-electric ships use ac distribution systems, the penetration of power electronic converters into power systems is giving rise to a tendency towards dc distribution systems [4–6]. The incentive for this transition lies on the one hand in the challenges associated with the conventional ship ac power systems, and on the other hand, in an increasing interest in integration of energy sources and storage devices with dc outputs [5,7]. The challenges of the conventional shipboard ac systems include the need for synchronization of the generation units, reactive power flow, inrush currents of transformers, harmonic currents, and three-phase imbalances. Fig. 1 shows single line diagram overview of a shipboard ac power system in comparison with that of a shipboard dc network. As the bulky ac switchgears and transformers are removed in the shipboard dc grids, the dc systems provide advantages such as space and weight savings, and flexible arrangement of equipment [8]. Not requiring synchronization of generation units, a dc power system enables the prime movers to operate at their optimal speeds, leading to significant fuel saving. Fig. 1 also shows that the dc system eliminates the need for multiple stages of conversion and

* Corresponding author. Tel.: +47 735 94242.
*E-mail addresses:* bijan.zahedi@ntnu.no, bijan.zahedi@gmail.com (B. Zahedi).

0378-7753/$ – see front matter © 2014 Elsevier B.V. All rights reserved.
http://dx.doi.org/10.1016/j.jpowsour.2014.01.031

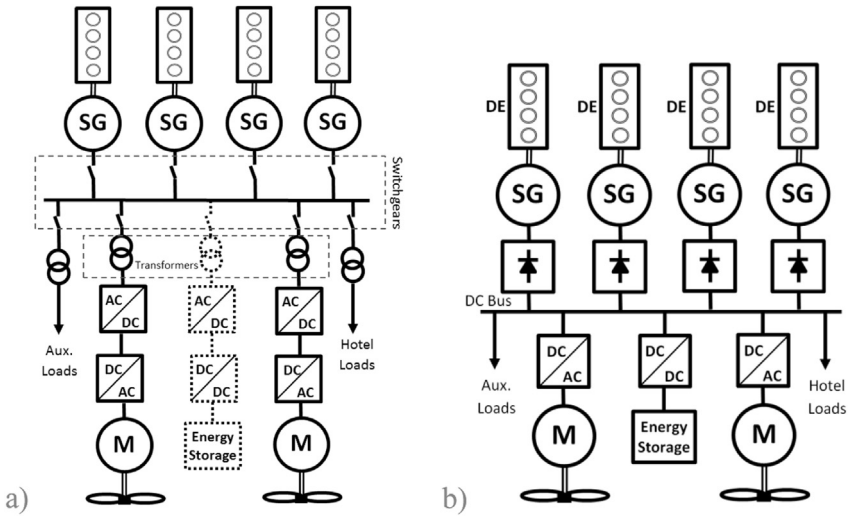


**Fig. 1.** Single-line diagram overview of shipboard power systems, a) ac network, b) dc network.

transformation that the ac system usually requires when integrating a device with dc output, such as an energy storage device.

Despite the long history of hybridization and fuel saving practices in land vehicles [9–19], marine hybrid-electric vessels are almost at the beginning of their journey, particularly with regard to integration of energy storage [6,20–28]. Presently, dc hybrid power systems are being considered for certain categories of ships that experience frequent load variations and/or long time of operation under non-rated conditions. Offshore Support Vessels (OSVs) form a major category of interest [8,24]. The first OSVs with dc power systems were delivered in 2012, including "Jaguar" with a power system from Alewijnse [29]. ABB and Siemens will launch OSVs with dc power systems in the current year. "Edda Ferd" introduced by Siemens will be the first OSV with a dc hybrid power system which benefits from variable-speed diesel engines and batteries, and assures a significant fuel saving compared to the conventional diesel-electric systems.

Although extensive research has been reported on efficiency optimization of hybrid electric vehicles [30–33], this issue for all-electric ships has largely remained unaddressed, leading to the research reported in this article. This paper is aimed at efficiency analysis and optimization of shipboard power systems and evaluation of their fuel saving when utilizing the dc distribution and incorporating an energy storage device. In Section 2, fuel consumption of the prime mover is discussed and modeled. The efficiency of the electrical sources, converters, and the energy storage are analyzed and modeled. In order to evaluate potential fuel saving by this system, in Section 3, an optimization algorithm is proposed for ship applications where multiple generator sets should be optimized in terms of their average powers and power ripples. The optimization algorithm extends the work of [34] that suits HEVs with a single generator, to all-electric ships running on multiple generator sets. The optimization algorithm minimizes the fuel consumption by optimal power sharing among the energy storage and prime movers. In Section 4, an online optimization strategy based on the proposed algorithm is applied to an offshore support vessel with seven different operational modes. MATLAB/Simulink is used to simulate the system. The control performance deficiencies resulted from the potential approximations of the online control is taken into account to more realistically estimate the optimized fuel saving onboard an actual vessel. The simulation results of the online optimization control are presented and compared with those of theoretical optimization algorithm. In Section 5, the conclusions of the study are drawn. The study results show substantial fuel saving for the optimally controlled dc hybrid power system in comparison with the conventional ac system and also with the dc system without energy storage.

## 2. Efficiency analysis and modeling

Fig. 2 depicts the architecture of the studied dc power system in more detail. The power system consists of four generation units, an energy storage system based on Li-Ion batteries, propulsion loads, ship service loads, and auxiliary loads. In each generation unit, a prime mover is coupled to a wound-rotor synchronous generator. The ac power of the generator is converted to dc power through a three-phase diode rectifier. The rotational speed of the prime mover is adjusted by a local controller to minimize fuel consumption. This is not possible in conventional ship ac power systems wherein the speed reference is constant to maintain synchronization among generators. In order to manage power sharing among generators while regulating the dc voltage level, the exciters of different generation units can be coordinated by voltage droop with secondary level control. The energy storage system consists of a Li-Ion battery bank and a bidirectional dc–dc converter that enables to charge and discharge the battery in a controlled manner.

In this section, the generation units are analyzed and modeled in terms of fuel consumption of the prime movers, and efficiency of the generator–rectifier systems. The efficiencies of the battery bank and the dc–dc converter are also analyzed and modeled. As the electrical load profile of the studied system is available, the efficiency models of the system loads are not required.

### 2.1. Prime mover

The main source of power onboard an all-electric ship typically comprises a synchronous generator, driven by an internal combustion engine (ICE) that is often fueled with diesel or heavy fuel oil [1]. The specific fuel consumption curves for an ICE, obtained from engine efficiency maps, have the qualitative behavior of Fig. 3 [7]. The combustion engines are continuously being improved regarding efficiency and emissions; however, their optimum utilization factor of fuel is still around 40%, and the rest of the stored energy in the fuel is dissipated through heat or the exhaust.

As seen in Fig. 3, the fuel utilization of an ICE can be improved by adjusting the engine speed based on the engine load. This implies a

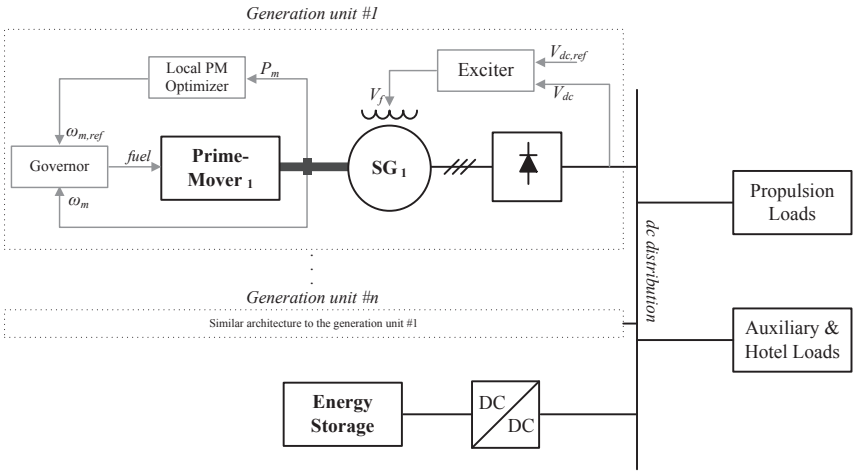


**Fig. 2.** Detailed architecture of the shipboard dc power system under study.

disadvantage of the conventional shipboard ac power systems, wherein all generator sets must be synchronized at a fixed frequency, preventing from the optimized speed control. A dc power system, however, enables the engines to rotate independently, bringing about the possibility of optimal speed adjustment. In ac power systems, independent rotation of the engines could be also provided by use of back-to-back converters for each generator. Nevertheless, this imposes more cost and complexity in comparison with the transition to the dc system. In addition, considerable ship electrical power is converted to dc to be used by the ship propulsion drives, which are the major loads in many applications. The use of back-to-back converters adds to the conversion stages between ac and dc, which reduces the drivetrain efficiency. Therefore, the dc system has become more appealing to the ship industry with regard to fuel saving.

The hourly fuel consumption curve for an ICE can be approximated by a quadratic function of the load as expressed in (1). This equation is valid for either variable-speed, or fixed-speed operation, using different sets of polynomial coefficients [34].

$$C_1 = C_0 + aP_m + bP_m^2. \tag{1}$$

where $C_0$, $a$, and $b$ are the coefficients of the second-order polynomial function, and $P_m$ is the engine mechanical power. The support points for the specific fuel consumption of a 300 kW diesel

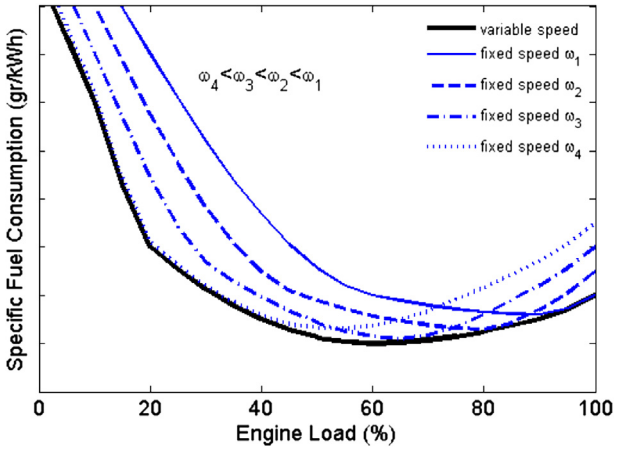


**Fig. 3.** Specific fuel consumption of an ICE.

engine are given in the Appendix [see 1.a)] under both variable and fixed-speed operations. The specific fuel consumption is the hourly consumption per unit of power, which is obtained by

$$\mathrm{SFC} = C_0/P_m + a + bP_m. \tag{2}$$

The above relations of fuel consumption also hold in dynamic conditions [34].

### 2.2. The synchronous generator–rectifier system

In a shipboard power generation system, the prime mover is coupled to an electric machine, typically a synchronous generator, to convert the mechanical energy into the electrical form. When dc distribution is considered, the three-phase ac power is to be converted to dc power through three-phase rectifiers. As bidirectional power flow is not required in such an application, three-phase diode rectifiers are appealing options due to their structural simplicity, high energy efficiency, and low cost. They can readily be used with wound-rotor synchronous generators [4,6].

Three-phase rectifiers are already used in the conventional electric propulsion systems to supply the dc links of propulsion electric drives. The transition from ac to dc can be viewed as the enhancement of these dc links to form a distributed dc bus, which leads to elimination of bulky ac switchboards, ac transformers, and their associated power losses [7]. In addition, it will be shown in the following that the efficiency of the generator is improved, when the prime mover is controlled at its optimal speed.

The main losses of the synchronous generator consist of copper losses, iron losses, and mechanical losses. The copper losses are resulted from the flow of current through the stator and rotor windings, which are calculated by

$$P_{Cu} = r_s I_s^2 + r'_{fd} I'^2_{fd} = r_s\left(i_{sd}^2 + i_{sq}^2\right) + r'_{fd} i'^2_{fd}. \tag{3}$$

where conventional notations are used. The iron losses are composed of eddy and hysteresis losses, which can be obtained by the following formula [35]

$$P_{Fe} = c_{Fe}\omega_e^{\beta}\lambda_m^2 = c_{Fe}\omega_e^{\beta}\left(X_{md}^2 i_{md}^2 + X_{mq}^2 i_{mq}^2\right). \tag{4}$$

where $\beta = 1.5$–$1.6$. This formula is represented in the machine equivalent circuit by the core resistance $R_c$ in parallel to the magnetizing reactors $X_{md}$ and $X_{mq}$. The mechanical losses are due

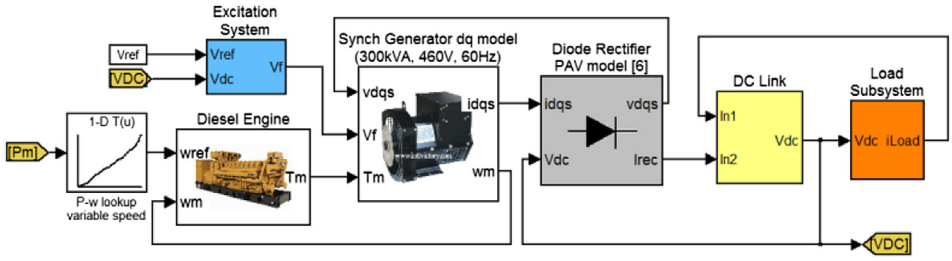


**Fig. 4.** Overview of the variable-speed control of a diesel–generator unit.

to friction and air drag losses, which are proportional to the square of rotational speed.

$$P_{l,m} = c_m \omega_m^2. \quad (5)$$

Power losses in diode rectifiers are mainly resulted from the conduction losses, and their switching losses are negligible. The conduction losses are given by

$$P_{rec} = 2V_{fw}I_{dc} + \frac{2}{3}R_{D,on}F_I^2 I_{dc}^2. \quad (6)$$

where $V_{fw}$ is the diode threshold voltage, and $F_I$ is the current waveform factor, which can readily be calculated for the typical diode current waveforms by $F_I = I_{D,rms}/I_{D,avg}$. Assuming that each diode has a half-sine current waveform, we calculate $\pi/2$ for the current waveform factor.

In order to evaluate the power losses in the generator–rectifier system and to obtain its efficiency curve, the simulation platform introduced in Ref. [6] is employed. The losses are investigated over a wide range of load for two conditions: 1) when engine speed is fixed at its rated value, and 2) when engine speed is optimally adjusted to consume minimum fuel. Fig. 4 shows the overview of the variable-speed control for one diesel engine. The optimal speed against the engine load can be deduced from the engine manufacturer's datasheet. For constant-speed operation, the reference speed is fixed at its rated value. The parameters of the diesel–generator sets are given in the Appendix [see 2)].

Fig. 5 depicts power loss components of the generator–rectifier system under fixed speed operation, while Fig. 6 shows the same components when the speed is varied to attain minimum SFC. In comparison of the two figures, it is observed that the generator core and mechanical losses reduce in variable-speed operation, while the copper losses slightly increase. Nevertheless, the total loss reduction outweighs the increase in copper losses, which results in higher efficiencies in variable-speed operation. Fig. 7 depicts the efficiency in the two operation modes, wherein the difference of the two efficiency curves increases as the load decreases.

The specific fuel consumption is calculated in terms of electrical load by using the efficiency curves of Fig. 7 and the SFC relation in (2). Fig. 8 depicts the curves of these new SFC relations for fixed and variable-speed operation, which are fitted to quadratic functions with coefficients given in the Appendix [see 1.b)]. These quadratic functions will be used in the development of the optimization algorithm.

### 2.3. The bidirectional dc–dc converter

In a dc hybrid power system, an energy storage device is prominent to improve the transient performance of the system, and to enable optimal load sharing among the sources. A bidirectional converter is normally used to incorporate the energy storage in the power system. Various topologies of bidirectional dc–dc power converters are discussed and compared in Refs. [36,37]. Topological circuit of a full-bridge bidirectional converter is depicted in Fig. 9. The high frequency transformer is used to provide high voltage transfer ratio to link a low voltage battery to the dc bus. The additional cost and losses introduced by the high frequency transformer can be justified when the voltage ratio between LV and HV is so high that devices are not economical to tolerate both high voltage and high current simultaneously [36]. The advantage of the full-bridge topology is to provide lower voltage and current stresses, resulting in significant decrease in losses compared to half-bridge and push–pull topologies [36]. Nevertheless, it needs high number of switches. The power losses of the converter of Fig. 9 for its two modes of operation are discussed in the following. The parameters of the studied converter are given in the Appendix [see 3)].

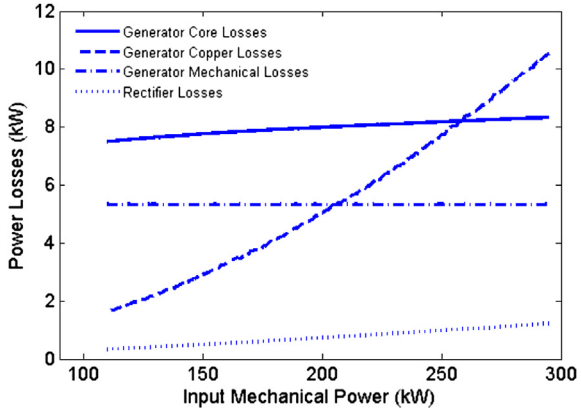


**Fig. 5.** Power losses of the generator–rectifier under fixed-speed operation.

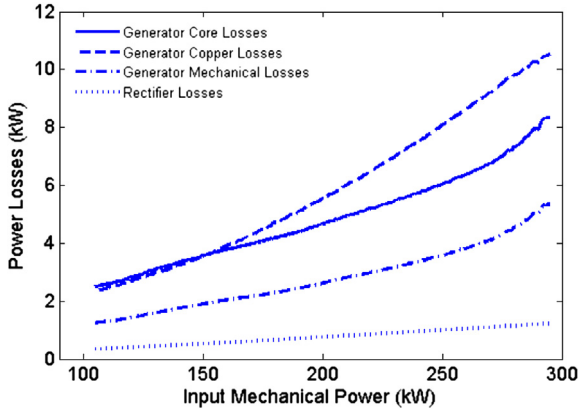


**Fig. 6.** Power losses of the generator–rectifier under adjusted-speed operation.

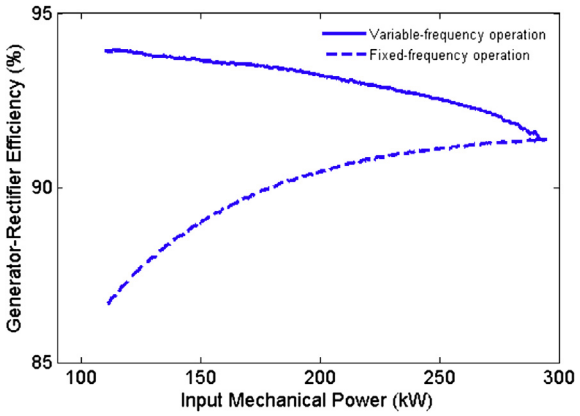


**Fig. 7.** Efficiency curves of the generator-rectifier under fixed and variable-speed operation.

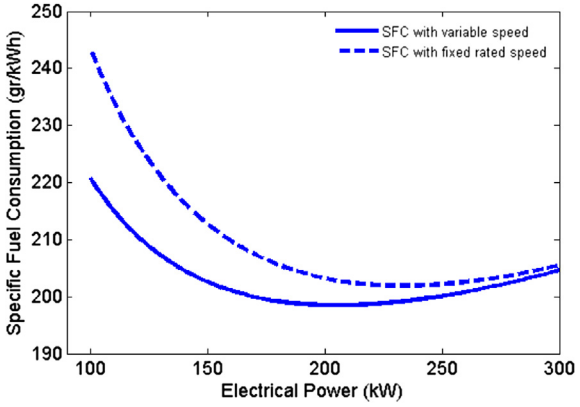


**Fig. 8.** SFC curves of the diesel–generator set in terms of electrical power under fixed and variable-speed operation.

The converter losses are comprised of the conduction and the switching losses of the transistors, the conduction losses of the diodes, and the resistive losses of the inductor, the transformer, and the capacitors. The transformer core losses are neglected, as the switching frequency is relatively low. In the following, the converter losses in buck mode are formulated. The losses are preferably derived in terms of HV-side power so as to provide an efficiency curve against exchanged power with the dc bus. Interested readers are referred to Ref. [38]-Ch. 3 for details on the derivation.

The transistors conduction losses are obtained by (7), assuming that the inductor current is ripple-free.

$$P_{\mathrm{Sw,on}} = R_{\mathrm{S,on}} I_{\mathrm{S,rms}}^2 = R_{\mathrm{S,on}} \left( \frac{P_{\mathrm{hv}} \sqrt{D}}{V_{\mathrm{hv}}} \right)^2. \tag{7}$$

Assuming that the transistor output capacitance is linear, we can calculate the switching losses by

$$P_{\mathrm{Sw,sw}} = 4 \left( \frac{f_{\mathrm{sw}}}{2} \right) C_{\mathrm{O}} V_{\mathrm{SM}}^2 = \frac{1}{2} f_{\mathrm{sw}} C_{\mathrm{O}} V_{\mathrm{hv}}^2. \tag{8}$$

The following equations hold for the diode conduction losses over a switching period.

$$p_{\mathrm{D}} = \begin{cases} V_{\mathrm{fw}} i_{\mathrm{L}} + 2R_{\mathrm{D,on}} i_{\mathrm{L}}^2, & (0 \le t \le DT) \\ V_{\mathrm{fw}} i_{\mathrm{L}} + (2R_{\mathrm{D,on}} \| 2R_{\mathrm{D,on}}) i_{\mathrm{L}}^2, & (DT \le t \le T) \end{cases} \tag{9}$$

Taking an average over the switching period, it yields

$$\begin{aligned} P_{\mathrm{D}} &= V_{\mathrm{fw}} I_{\mathrm{L}} + R_{\mathrm{D,on}} I_{\mathrm{L}}^2 D + 2R_{\mathrm{D,on}} I_{\mathrm{L}}^2 (1 - D) \\ &= V_{\mathrm{fw}} \left( \frac{nP_{\mathrm{hv}}}{DV_{\mathrm{hv}}} \right) + (2 - D) R_{\mathrm{D,on}} \left( \frac{nP_{\mathrm{hv}}}{DV_{\mathrm{hv}}} \right)^2. \end{aligned} \tag{10}$$

The resistive losses of the passive elements are obtained by

$$P_{\mathrm{L}} = r_{\mathrm{L}} I_{\mathrm{L,rms}}^2 = r_{\mathrm{L}} \left( \frac{nP_{\mathrm{hv}}}{DV_{\mathrm{hv}}} \right)^2. \tag{11}$$

$$P_{C1} = r_{C1} I_{C1,\mathrm{rms}}^2 = r_{C1} \left( \frac{(1 - D) P_{\mathrm{hv}}}{DV_{\mathrm{hv}}} \right)^2. \tag{12}$$

$$P_{C2} = r_{C2} I_{C2,\mathrm{rms}}^2 = r_{C2} \left( \frac{(1 - D) V_{\mathrm{lv}}}{\sqrt{12} f_{\mathrm{sw}} L} \right)^2. \tag{13}$$

$$P_T = r_T I_{T,\mathrm{rms}}^2 = r_T \left( \frac{nP_{\mathrm{hv}}}{V_{\mathrm{hv}} \sqrt{D}} \right)^2. \tag{14}$$

The power loss components in buck mode are depicted in Fig. 10, using the above formulas. Analysis of the boost mode is carried out in a similar way to the above formulation, and results in the loss components depicted in Fig. 11. For consistency, the formulas for boost mode are summarized in the Appendix [see 4)].

Fig. 12 shows the converter efficiency curves for the two modes, which are slightly different. A simplified model of the converter losses is desired for the analysis of optimal conditions discussed later in the paper. Therefore, an averaged efficiency curve between the two modes is considered, as the converter is equally operated in both modes to sustain the battery charge level. The converter losses, thereafter, can be modeled by an equivalent resistance, as

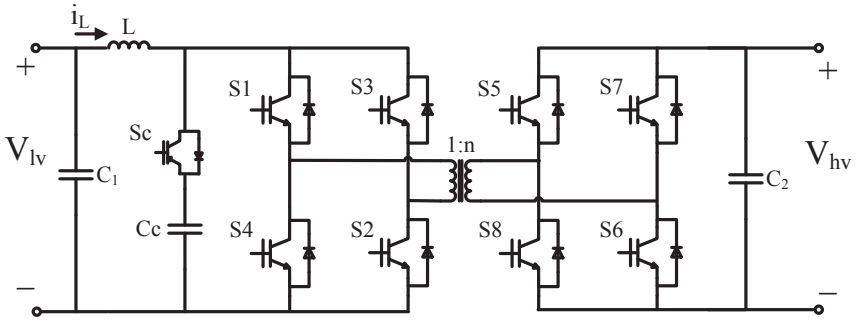


**Fig. 9.** The topological circuit of the full-bridge bidirectional dc–dc converter under study.

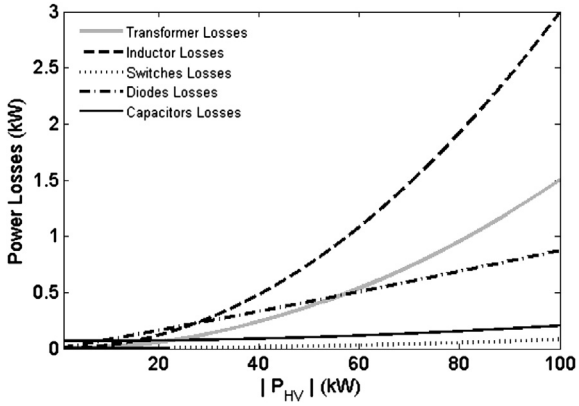


**Fig. 10.** The power loss components of the bidirectional converter in buck mode.

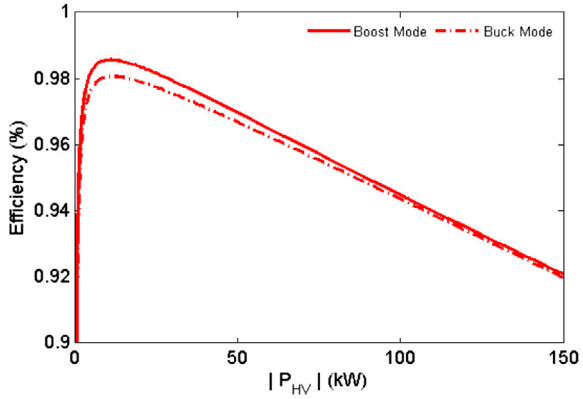


**Fig. 12.** Efficiency curves of the bidirectional converter in buck and boost modes.

expressed by (15). This equation also includes a small constant term, resulted from constant switching losses, and capacitor losses. As seen in Fig. 13, the loss model of (15) complies with the detailed converter losses.

$$P_{\mathrm{l,bid}} = \frac{R_{\mathrm{bid}}}{V_{\mathrm{bus}}^2} P_{\mathrm{hv}}^2 + P_{l0}. \tag{15}$$

$R_{\mathrm{bid}}$ is the equivalent resistance of the bidirectional converter. In order to provide a total loss model of the energy storage system, battery losses can be integrated in the converter loss model as discussed in the following.

### 2.4. The battery model

To develop an optimization control strategy, using a reference model of the battery is essential. Electrochemical battery models [39–41] can often provide high accuracy by capturing all key behaviors of the electrochemical cells. However, being based on partial differential equations with large number of unknown parameters, they could lead to unnecessary complex models for the purpose of power management control.

Equivalent circuit battery models have been widely used for the purpose of power management studies. They are lumped models with relatively small number of parameters. [42] studies a number of these equivalent circuit models for Li-Ion batteries. As the battery SOC in the current research is maintained within a narrow range of high SOC values, the simple model presented in Ref. [42] is chosen. This simple model is a SOC-dependent voltage source in series with an equivalent resistance.

The above-mentioned simple model is used only for the analytical derivation of the optimization strategy. However, for the system simulation, the battery model of the Simulink library is used. The details of the Simulink battery model can be found in Ref. [43]. The internal resistance of a Li-Ion battery bank rated at 80 V and 1000 Ah is 0.8 mΩ which is calculated through the user interface of the Simulink model. Such a small value of resistance is resulted from a high number of parallel branches of battery cells to provide the required capacity.

The battery loss model, based on its equivalent resistance "$R_{\mathrm{b}}$", is readily integrated in (15) by

$$P_{\mathrm{l,ess}} = \frac{R_{\mathrm{ess}}}{V_{\mathrm{bus}}^2} P_{\mathrm{hv}}^2 + P_{l0}. \tag{16}$$

where $R_{\mathrm{ess}}$ is the equivalent resistance of the energy storage system that is expressed by

$$R_{\mathrm{ess}} = R_{\mathrm{bid}} + \frac{n^2}{(1-D)^2} R_{\mathrm{b}}. \tag{17}$$

The above simplified model of the energy storage system is helpful in development of the optimization algorithm that will be discussed in the next section.

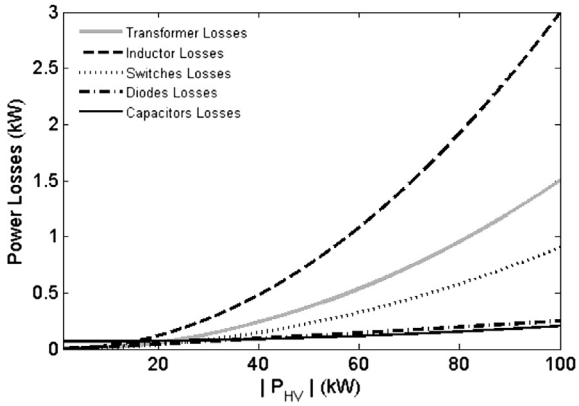


**Fig. 11.** The power loss components of the bidirectional converter in boost mode.

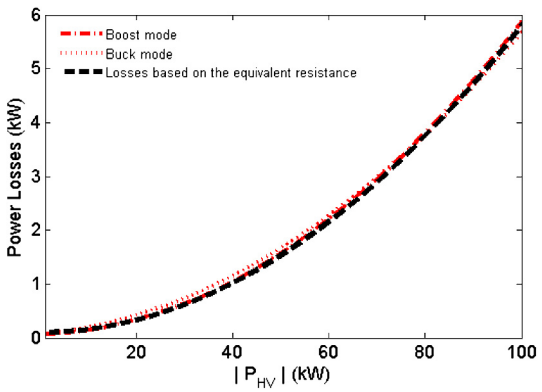


**Fig. 13.** The converter losses based on the equivalent resistance.

## 3. Optimization algorithm

The presence of more sources of power causes more complexity in power management, calling for an effective strategy to coordinate the sources properly and to make an appropriate choice among different possible alternatives. Various control strategies can be devised in a hybrid power system so as to achieve desired performance goals, optimized energy efficiency, reduced emission, or improved reliability and safety. This section deals with optimization of energy efficiency, which is discussed in the following.

Fig. 14 compares fuel consumption of a shipboard dc power system with that of a conventional shipboard ac power system. The solid curves depict specific fuel consumption for the dc power system of Fig. 1, wherein "$k$" active diesel engines are controlled at their optimal speeds. This set of active generation units of the dc power system will be called "dc source" hereafter in this paper. The dotted curves depict specific fuel consumption for a conventional ac power system, wherein the same set of diesel-generators of Fig. 1 is used, and "$k$" active diesel engines operate at fixed speed. Besides the comparison, Fig. 14 also implies how the replacement of a high-power generation unit with a set of low-power generation units results in substantial fuel saving, especially under light-load conditions. In addition, it yields a quantitative measure to determine the optimal number of active generator sets based on the system load. However, more considerations exist with regard to optimization, which are discussed here in this section.

In practice, potential large transients of the ship electrical load may require the system to continuously keep a redundant active generator set. This is already a technical requirement for several ship types including OSVs, which leads to considerable increase in their fuel consumption. In case an energy storage device is integrated in the system, it can supply the transient power until an engine start-up is really necessary. This would provide the required redundancy with no additional fuel consumption [24].

The energy storage also enables the engines to operate at their optimal conditions. It is apparent in Fig. 14 that the optimal fuel consumption is achieved when the engines are operated at their minimum SFC point. However, due to power losses of the energy storage, the optimal operation is not necessarily achieved by keeping the engine operating point at the minimum SFC. A compromise is to be considered between the minimum engine SFC and the maximum efficiency of the energy storage system. Besides, existing ripple of the generator load causes ripples on the engine SFC that results in additional fuel consumption. Therefore, the power ripple of the generation units should also be optimized. This will be discussed in detail later in this section.

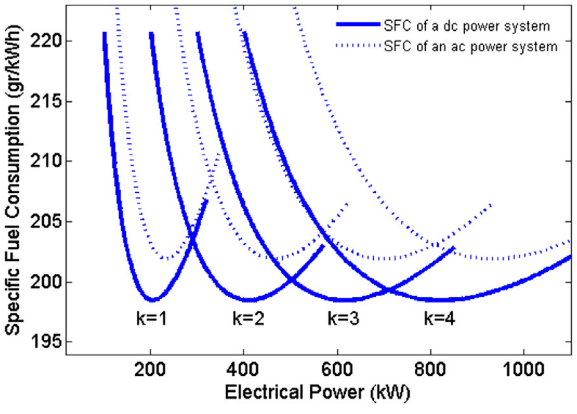


**Fig. 14.** SFC curves for "$k$" active diesel engines in a dc power system compared to those in the conventional ac power system.

According to the above discussion, the optimization strategy has two main tasks: first, to calculate the optimal value for the average power of the dc source, and second, to find the optimal value for the power ripple of the dc source. This section extends the work of [34] to suit the multi-generator shipboard power system of Fig. 1.

The power of the dc source is expressed in terms of an average value and a ripple proportional to the load ripple.

$$P_s(t) = P_{sa} + \alpha(P_L(t) - P_{La}) \quad (0 \le \alpha < 1). \tag{18}$$

where $P_{sa}$ and $P_{La}$ are the averaged values of the dc source power and the load respectively, and $\alpha$ determines the fraction of the load ripple supplied by the dc source. The rest of the load ripple is to be supplied by the battery, which is also loaded by an averaged power of $P_{La} - P_{sa}$. The purpose of the following analysis is to find optimal values for $P_{sa}$ and $\alpha$.

### 3.1. Charge–discharge mode

In order to maintain the state of charge (SOC) of the battery within a certain limit, it is required that a diesel generator starts when SOC reaches the lower boundary, and shuts down as soon as SOC exceeds the upper limit. Therefore, two operating modes can be considered for the dc source, which are addressed here by charge mode and discharge mode. We rewrite (18) for the two modes of discharge and charge respectively.

$$P_{s,k}(t) = P_{sa,k} + \alpha_k(P_L(t) - P_{La}) \quad (0 \le \alpha_k < 1). \tag{19}$$

$$P_{s,k+1}(t) = P_{sa,k+1} + \alpha_{k+1}(P_L(t) - P_{La}) \quad (0 \le \alpha_{k+1} < 1) \tag{20}$$

where $k$ is the number of active engines in discharge mode. Fig. 15 shows an overview of the optimization problem. In this figure, the system is supplying a load with an average of $P_{La}$ and ripple amplitude of $\hat{P}_L$. Charging and discharging the energy storage periodically, we can move the operating point toward lower SFCs. During the charge mode, "$k+1$" active engines supply the load while charging the battery with $P_{ch,a}$. This moves the operating point from point A to point B, reducing the SFC value. During the discharge mode, "$k$" engines are active and the battery is discharged with $P_{dis,a}$ in order to assist the generators to supply the load. The operating point, in this mode, moves to point B′. In order to find the optimal work points B and B′, the optimal average value of the dc source power can be calculated for both charge and discharge modes i.e. $P_{sa,k}$ and $P_{sa,k+1}$.

In addition, the power ripple of the dc source may also cause additional fuel consumption. It is seen in Fig. 15 that although the average of $P_{s,k}(t)$ is equal to $P_{sa,k}$, the average of SFC($P_{s,k}(t)$) is greater than SFC($P_{sa,k}$), which is resulted from the nonlinearity of SFC curves. This means that the power ripple may lead to additional fuel consumption, as the fuel consumption is proportional to the average of SFC over time. Thus, the power ripple of the dc source should be optimized as well as its average power.

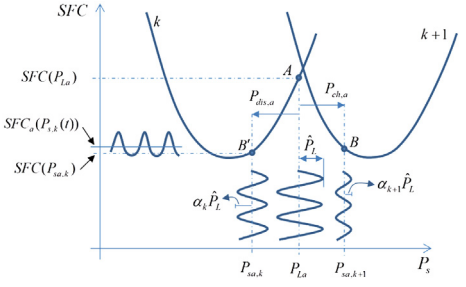


**Fig. 15.** Qualitative representation of the optimization problem.

Based on the foregoing discussion, the set of variables that must be optimized consists of $P_{sa,k}$, $P_{sa,k+1}$, $\alpha_k$, and $\alpha_{k+1}$. The solution of the optimization will be a compromise between the minimum consumption of the dc source, and the maximum efficiency of the energy storage system. The number "$k$", which is the number of active engines in discharge mode, is an integer between 0 and 3 for the system under study. It is determined in such a way that $P_{La}$ lies between the minimum SFC points of the two neighboring SFC curves.

Assuming that each charge/discharge cycle lasts for $T_c$, including a charge time $T_{ch}$ and a discharge time $T_{dis}$, we obtain the total fuel consumption by taking integral of (1) over time "$t$".

$$C(t) = N_{su}\Bigg\{C_{0,k+1}T_{ch} + a_{k+1}\int_{T_E} P_{s,k+1}(t)\mathrm{d}t + b_{k+1}\int_{T_{ch}} P_{s,k+1}^2(t)\mathrm{d}t + C_{0,k}T_{dis} + a_k\int_{T_{dis}} P_{s,k}(t)\mathrm{d}t + b_k\int_{T_{dis}} P_{s,k}^2(t)\mathrm{d}t + C_{su}\Bigg\}. \tag{21}$$

Considering the energy balance of the energy storage over a charge/discharge cycle, we can obtain the different time periods of $T_c$, $T_{ch}$, and $T_{dis}$ in terms of the other variables (Appendix [see 5.b)], which gives

$$C(t) = t\Bigg\{C_{0,k+1}D_s + C_{0,k}D_s' + aP_{La} + aD_s\frac{R_{ess}}{V_{bus}^2}\left[\left(P_{sa,k+1}-P_{La}\right)^2 + R_{eq}^2(1-\alpha_{k+1})^2\right] + aD_s'\frac{R_{ess}}{V_{bus}^2}\left[\left(P_{sa,k}-P_{La}\right)^2 + R_{eq}^2(1-\alpha_k)^2\right] + b_{k+1}D_s\left(P_{sa,k+1}^2 + \alpha_{k+1}^2R_{eq}^2\right) + b_kD_s'\left(P_{sa,k}^2 + \alpha_k^2R_{eq}^2\right) + \frac{C_{su}}{T_c}\Bigg\}. \tag{24}$$

where $D_s = 1 - D_s' = T_{ch}/T_c$is calculated by

$$D_s = \frac{P_{La} - P_{sa,k} + \frac{R_{ess}}{V_{bus}^2}\left[\left(P_{sa,k}-P_{La}\right)^2 + R_{eq}^2(1-\alpha_k)^2\right]}{P_{sa,k+1} - P_{sa,k} - \frac{R_{ess}}{V_{bus}^2}\left[\left(P_{sa,k+1}-P_{sa,k}\right)\left(P_{sa,k+1}+P_{sa,k}-2P_{La}\right) + R_{eq}^2(\alpha_{k+1}-\alpha_k)(\alpha_{k+1}+\alpha_k-2)\right]} \tag{25}$$

where $N_{su}$ is the number of engine start-ups over the time "$t$". An equivalent value for fuel consumption at each engine start-up is also considered which is represented by $C_{su}$.

The equivalent power ripple is defined by means of an integrative function "$R_{eq}$" that is expressed by

$$R_{eq} = \sqrt{\frac{1}{t}\int_t \left(P_L(t) - P_{La}\right)^2\mathrm{d}t}. \tag{22}$$

Taking the steps provided in the Appendix [see 5.a)], we can derive (23) from the integral terms of (21), which yields the fuel consumption as

$$C(t) = N_{su}\Bigg\{C_{0,k+1}T_{ch} + C_{0,k}T_{dis} + aP_{La}(T_{ch}+T_{dis}) + aT_{ch}\frac{R_{ess}}{V_{bus}^2}\left[\left(P_{sa,k+1}-P_{La}\right)^2 + R_{eq}^2(1-\alpha_{k+1})^2\right] + aT_{dis}\frac{R_{ess}}{V_{bus}^2}\left[\left(P_{sa,k}-P_{La}\right)^2 + R_{eq}^2(1-\alpha_k)^2\right] + b_{k+1}T_{ch}\left(P_{sa,k+1}^2 + \alpha_{k+1}^2R_{eq}^2\right) + b_kT_{dis}\left(P_{sa,k}^2 + \alpha_k^2R_{eq}^2\right) + C_{su}\Bigg\}. \tag{23}$$

The fuel consumption represented by (24) has a minimum that satisfies

$$\frac{\partial C}{\partial \alpha_k} = 0, \quad \frac{\partial C}{\partial \alpha_{k+1}} = 0, \quad \frac{\partial C}{\partial P_{sa,k}} = 0, \quad \frac{\partial C}{\partial P_{sa,k+1}} = 0. \tag{26}$$

Fig. 16 depicts the hourly fuel consumption of the dc power system under a certain load in terms of the dc source loading conditions. As the hourly fuel consumption has a five dimensional surface, it is drawn in terms of only one pair of $(\alpha, P_{sa})$ at each time, assuming the other pair to be fixed at$(\alpha^*, P_{sa}^*)$. Therefore, two separate graphs are used to depict the fuel consumption against the two pairs. The optimal values of $P_{sa,k}$, $P_{sa,k+1}$, $\alpha_k$, and $\alpha_{k+1}$ can numerically be obtained by searching for the minimum fuel consumption in the analytical relation (24).

### 3.2. Continuous mode

The obtained optimal loading conditions must also satisfy the limits on the engine duty cycle "$D_s$". The resulted duty cycle must be a value between 0 and 1; otherwise the dc source operates at a continuous mode. In case the resulted duty cycle is less than or close to zero, the dc source operates with "$k$" active diesel engines continuously, and if the duty cycle is greater than or close to one, the dc source continuously operates with "$k+1$" active engines.

In such conditions, the optimal values can be analytically attained by

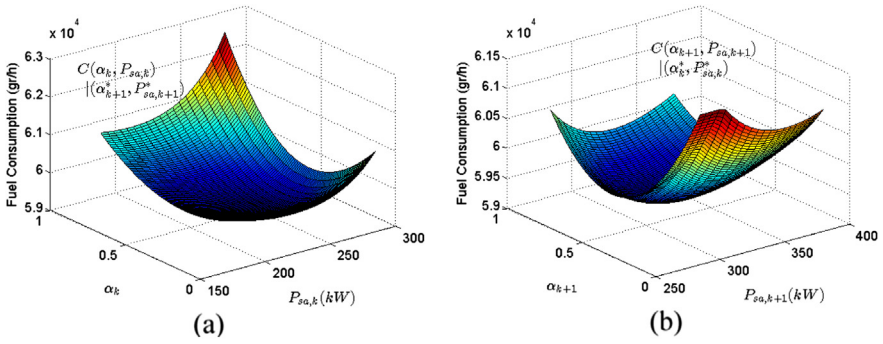


**Fig. 16.** Hourly fuel consumption of the dc source under a certain load, a) in terms of loading conditions in discharge mode, b) in terms of loading conditions in charge mode.

$$P_{\mathrm{sa},j} = P_{\mathrm{La}} + \frac{V_{\mathrm{bus}}^2}{2R_{\mathrm{ess}}} - \frac{1}{2}\sqrt{\frac{V_{\mathrm{bus}}^4}{R_{\mathrm{ess}}^2} - 4R_{\mathrm{eq}}^2\left(1-\alpha_j\right)^2}. \tag{27}$$

$$\alpha_j = 1 - \frac{b_j V_{\mathrm{bus}}^2/R_{\mathrm{ess}}}{\sqrt{4b_j^2R_{\mathrm{eq}}^2 + \left(a_j + 2b_jP_{\mathrm{La}} + b_jV_{\mathrm{bus}}^2/R_{\mathrm{ess}}\right)^2}}. \tag{28}$$

where $j = \begin{cases} k, & D_s \le 0 \\ k+1, & D_s \ge 1 \end{cases}$

In the following section, the presented algorithm will be used in an online optimization strategy for an offshore support vessel at its different modes of operation.

## 4. Online optimization strategy

The optimization algorithm presented in the previous section should be tailored to suit online computations and control. In the theoretical approach, analytical definitions for some variables are, as such, dependent on the future data of the system, for example the equivalent power ripple "$R_{\mathrm{eq}}$" and the average power $P_{\mathrm{La}}$. As future data is not available in online computations, these variables need to be estimated. In addition, the online processing requires reduced computational intensity to perform the tasks in real time. This can be provided by reducing the step sizes in online processing when searching for optimal values of $P_{\mathrm{sa},k}$, $P_{\mathrm{sa},k+1}$, $\alpha_k$, and $\alpha_{k+1}$. These estimations and simplifications may deteriorate the effectiveness of the method. In order to evaluate the performance of the method under online operation, this section presents the simulation results of the online control in comparison with those of the offline theoretical algorithm.

An online control, based on the theoretical algorithm is used in simulation of an offshore support vessel over a number of operational modes. The parameters of the system are reported in the Appendix. The power demands at each of the operating modes are specified in Table 1, where the number of active engines, average power, load fluctuation, and duration for each mode are given. These data are deduced from the experiences of ABB and DNV reported in Refs. [7,24].

For each mode of operation, the algorithm outputs the optimal loading conditions of the dc source, i.e. $P_{\mathrm{sa},k}$, $P_{\mathrm{sa},k+1}$, $\alpha_k$, and $\alpha_{k+1}$, and also the control mode (charge–discharge or continuous). The algorithm suggests the continuous mode when the operating point of the dc source is close to the minimum SFC; otherwise it suggests the charge–discharge mode as the optimal mode. While the offline algorithm uses a step-size of 0.01 in search for optimal $\alpha_k$ and $\alpha_{k+1}$, requiring 100 steps, the online algorithm uses a step-size of 0.05, which needs 20 steps. This provides significant reduction in computational intensity in search for optimal $\alpha_k$ and $\alpha_{k+1}$. The number of steps in search for $P_{\mathrm{sa},k}$ and $P_{\mathrm{sa},k+1}$ is considered 20 in both online and offline processing. Another difference between the offline algorithm and the online control is related to estimation of the load average "$P_{\mathrm{La}}$", and the equivalent power ripple "$R_{\mathrm{eq}}$". As the future data for these variables are not available, their online estimate can be obtained through filtering their instantaneous values by

$$P_{\mathrm{La}}(s) = \frac{1}{1+sT}P_{\mathrm{L}}(s). \tag{29}$$

$$R_{\mathrm{eq}}^2(s) = \frac{1}{1+sT}\left(P_{\mathrm{L}}(s) - P_{\mathrm{La}}(s)\right)^2. \tag{30}$$

where the filter time constant "$T$" should properly be chosen; A too short time constant causes unnecessary engine start-stops, when a change occurs in the load profile. A too long time constant causes that the dc source operates under non-optimal conditions for an unnecessary long period of time after a step change occurs in the system load. The choice of the time constant is critical considering that the load variations might have extremely low frequencies in ship applications, e.g. in low dynamic positioning mode. In order to adapt to various situations, two different time constants have been considered in the simulations. When a change happens in the load profile, e.g. changes in ship operating mode, the system selects the short time constant throughout the transition time to follow the load average quickly. In the normal operation at each mode, the control system uses the larger time constant that results in more efficient control. The mode transition is detected by observing a monotonic change in the load average for some seconds. Repeated simulations have shown that suitable values for the short and long time constants are 300 s and 1000 s respectively. Fig. 17 shows the simulation results of the optimized shipboard dc power system at three modes of harbor, high dynamic positioning, and transit supply. It is seen that in harbor and transit supply modes, one of the

**Table 1**
Parameters of the ship operating modes.

| Operating mode | # of active engines | $P_{\mathrm{La}}$ (%) | $P_{\mathrm{Lp}}$ (%) | Duration (h) |
|---|---|---|---|---|
| Low dynamic positioning (LDP) | 2 | 33 | 20 | 7.5 |
| High dynamic positioning (HDP) | 3 | 53 | 20 | 4 |
| Anchor handling (AH) | 3 | 50 | 2 | 1.5 |
| Harbor (H) | 1 | 17 | 1 | 1.5 |
| Bollard pull (BP) | 4 | 66 | 2 | 0.5 |
| Transit towing (TT) | 4 | 72 | 1 | 3 |
| Transit supply (TS) | 2 | 33.5 | 1 | 6 |

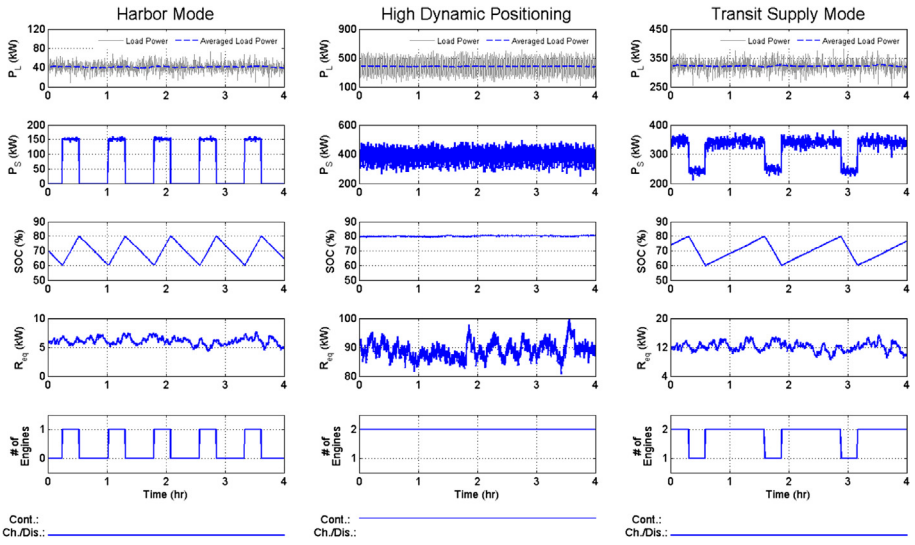


**Fig. 17.** Simulation results for three operating modes of the shipboard hybrid power system with online optimization.

diesel engines periodically turns on and off. This is the control mode that we earlier called "charge–discharge mode". The battery state of charge (SOC) is bounded between 60 and 80%. The energy storage system periodically charges and discharges with optimum average values, and also supplies an optimum fraction of the power ripple. In high dynamic positioning mode, in which the load average is close to the rated conditions, the system operates at "continuous mode", and the energy storage system only supplies an optimum fraction of the power ripple. At the bottom of Fig. 17, there is a flag indicating whether the control mode is "charge–discharge" or "continuous".

Simulation results over an operating cycle consisting seven different modes are presented in Fig. 18. The operating modes over the cycle are indicated on top of the figure. The upper plot shows the instantaneous and average load power. The dual time-constant characteristic of the filter is particularly clear in low dynamic positioning (LDP). At the beginning of the LDP mode, short after the mode transition, the average power follows the instantaneous value, as the smaller time constant is chosen. Thereafter, when the transition is completely over, the larger time constant is selected in order to filter the extremely low frequency variations. This procedure is carried out at all mode transitions.

During harbor, transit towing, and transit supply, the control system operates at charge–discharge mode, as periodical changes in the number of active engines and the battery SOC are seen. During the rest of ship operating modes, the control system operates at continuous mode, and the battery mainly contributes in supplying the power ripple.

Table 2 presents the optimized fuel consumption in comparison with non-optimized dc and ac systems. It also compares fuel consumption results for the online and the offline optimization methods at different ship operating modes. Regarding specific fuel consumption (SFC), two modes of AH and HDP have average power values of 400 kW which are in the proximity of the minimum SFC

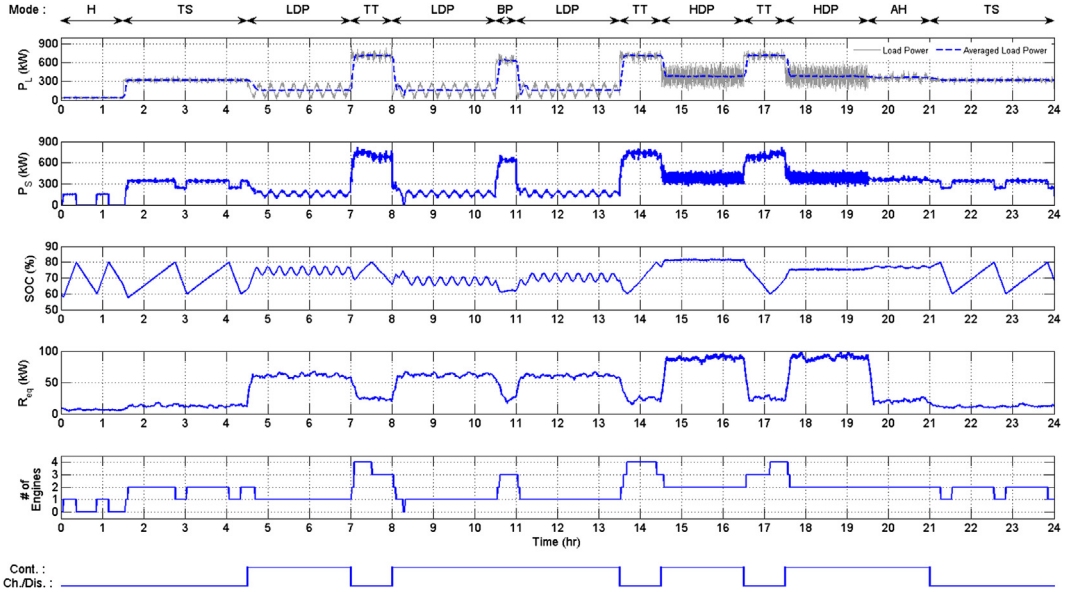


**Fig. 18.** Simulation results of the optimized shipboard hybrid power system over an operation cycle with 7 modes.

**Table 2**
Fuel consumption based on the algorithm and the simulation, compared to non-optimized systems.

| Operating mode | DC system with ESS (Optimized) | | | | | | | | DC system w/o ESS | AC system |
|---|---|---|---|---|---|---|---|---|---|---|
| | Control mode | # of active engines | $P_{sa,k+1}$ (%) | $P_{sa,k}$ (%) | $\alpha_{k+1}$ | $\alpha_k$ | $C_{opt}$ (gr/h) (algorithm) | $C_{opt}$ (gr/h) (simulation) | $C_{DC}$ (gr/h) | $C_{AC}$ (gr/h) |
| LDP | Cont. | 1 | 66.0 | N/A | 0.39 | N/A | 3.19E+04 | 3.32E+04 | 3.79E+04 | 4.32E+04 |
| HDP | Cont. | 2 | N/A | 79.0 | N/A | 0.49 | 7.59E+04 | 7.69E+04 | 7.95E+04 | 8.51E+04 |
| AH | Cont. | 2 | N/A | 75.0 | N/A | 0.49 | 7.17E+04 | 7.22E+04 | 7.58E+04 | 8.17E+04 |
| H | Ch./dis. | 1/0 | 62.8 | N/A | 0.36 | N/A | 9.83E+03 | 1.16E+04 | 1.35E+04 | 1.69E+04 |
| BP | Cont. | 3 | N/A | 75.3 | N/A | 0.78 | 1.26E+05 | 1.27E+05 | 1.28E+05 | 1.33E+05 |
| TT | Ch./dis. | 4/3 | 77.2 | 94.6 | 0.77 | 0.72 | 1.38E+05 | 1.38E+05 | 1.38E+05 | 1.43E+05 |
| TS | Ch./dis. | 2/1 | 71.2 | 100 | 0.61 | 0.44 | 6.47E+04 | 6.50E+04 | 7.64E+04 | 8.68E+04 |

(see Fig. 14). One may argue that the loading points of this study have by chance fallen in inefficient regions so that the resulted improvement from the control system would be unrealistically high. Although the load profile is based on actual data reported in Refs. [7,24], to include more efficient modes, we also study two modes that are shifted to the minimum SFC point rated at 800 kW. Let call these modes high Bollard Pull (HBP) and High Transit Towering (HTT). In case the two modes BP and TT are replaced with HBP and HTT respectively, 4 out of 7 operational modes are in the proximity of minimum SFC according to Fig. 14. The simulation results for these two modes are shown in Fig. 19. It is seen that under this loading condition, four diesel engines operate in continuous mode, and the battery only contributes in supplying the power ripple. The optimized fuel consumption is 1.526e+5 (gr/h), which is exactly the same as that of the dc system without energy storage. Therefore, the energy storage cannot provide any fuel saving for the dc system in these modes. However, the fuel consumption of the ac system is 1.567e+5 (gr/h) under the same loading condition. This means 2.6% fuel saving is still provided by the optimized system compared to the conventional ac system. These fuel saving results will also be used later in the concluding evaluations of this section.

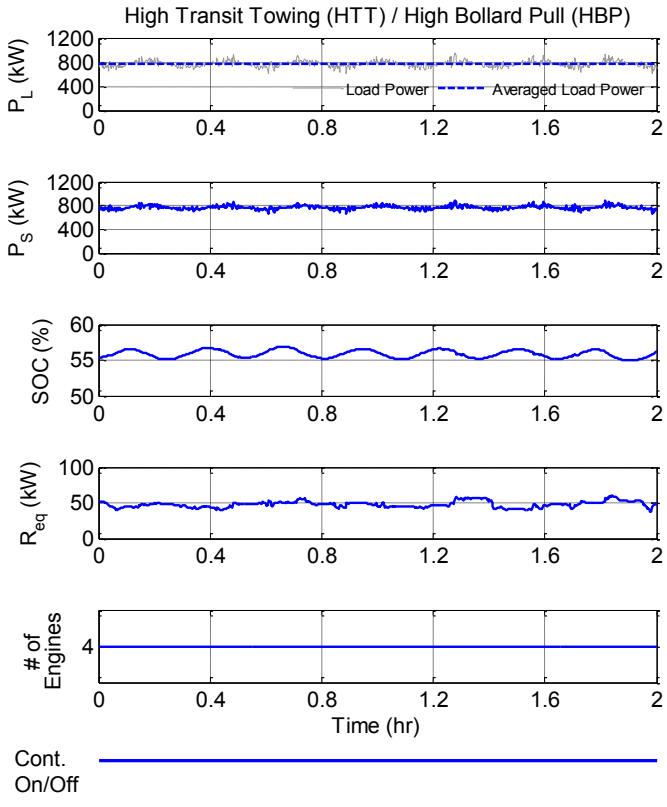


**Fig. 19.** Simulation results for the modes HBP and HTT of the dc hybrid power system with online optimization.

The fuel consumption of the simulation is slightly higher compared to the algorithm, which is caused by estimations of (29) and (30) as well as the step-size reductions in search for the optimal loading conditions. The fuel saving achieved by the optimization method is shown in percentage in Fig. 20. The optimization method provides more fuel saving in those modes whose power demand is away from the rated conditions. These modes include harbor, transit supply, and low dynamic positioning modes. Due to approximations made in the online optimization, the resulted fuel saving of the simulation is less than that of the algorithm by around 1% in average. The difference between the performances of the simulation and the algorithm peaks at harbor mode. This is mainly resulted from the steep SFC characteristic over the low-power range which the harbor mode belongs to. This makes the harbor mode more sensitive to the errors resulted from the approximations of the online processing. However, due to the low-power characteristic of the harbor mode, it has a minor effect on the overall performance of the online control.

The presented results in Fig. 20 show an average fuel saving of 15.3% for online control simulation when the conventional shipboard ac power system is replaced by a dc hybrid power system. This percentage is calculated based on weighted averaging of consumed fuel of the seven different operating modes. The system simulation over the 24-h cycle results in even a slightly higher fuel saving of 15.8%.

Fig. 20 also shows that integration of an energy storage system into the dc power system can provide a fuel saving of 7.3%. In case the modes HBP and HTT are considered instead of BP and TT respectively, the average fuel saving would be 14.6% compared to the conventional ac power system, and 7.0% compared to the dc system without energy storage. It should be noted that a noticeable part of fuel saving is resulted from optimizing the number of active generation units. As addressed in Section 3, the conventional OSVs are required to continuously keep a redundant active engine during most modes of operation [see Table 1]. However, the onboard energy storage of a hybrid power system, while optimizing the loading conditions of the engines, plays the role of a redundant active engine that enables optimization of the number of active engines as well. Therefore, the achieved fuel saving is resulted partly from optimization of the number of active engines and partly from optimization of loading conditions of the diesel–generators. The study results demonstrate a significant potential regarding fuel saving in offshore support vessels through transition from ac to dc power systems and integration of energy storage devices. The fuel saving potential is not limited to the studied type of ships, but can

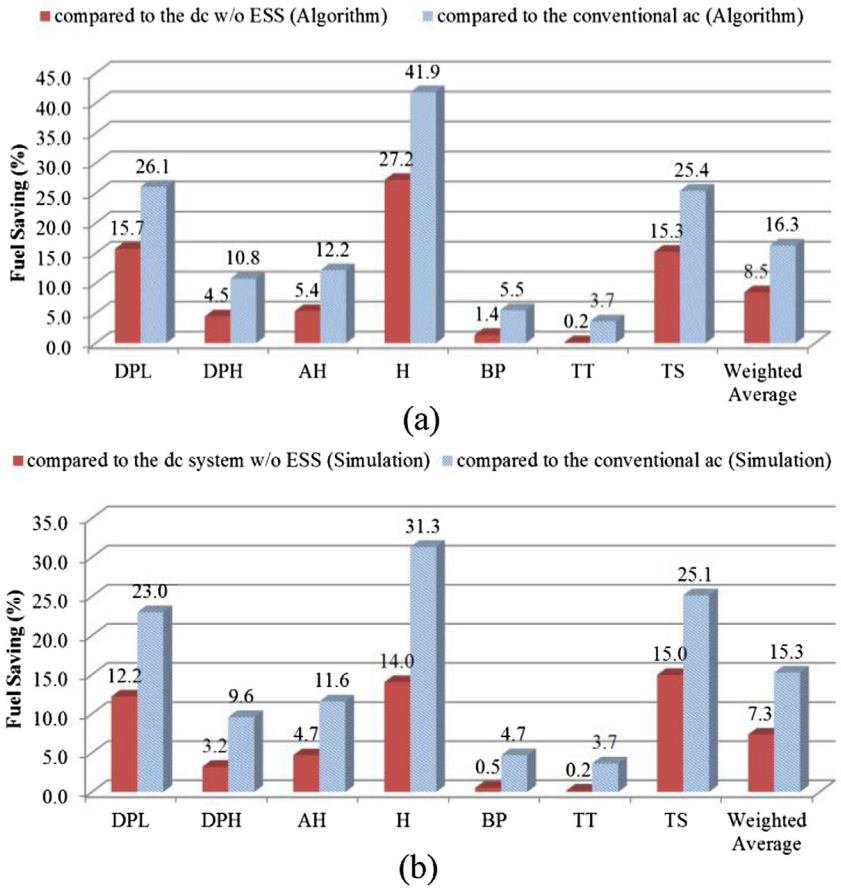


**Fig. 20.** Resulted fuel saving from the optimization strategy, a) algorithm results, b) online simulation results.

be also considered for a wide range of marine vessels that have frequent load variations or long-time operation under non-rated conditions.

## 5. Conclusion

In this paper, detailed efficiency analysis of a shipboard dc hybrid power system was carried out in order to evaluate its potential fuel saving. It was shown that maximum fuel saving conditions for such a system required the generator sets to operate at optimal loading conditions in terms of average power and power ripple. A numerical optimization algorithm was proposed to find optimal loading conditions, using the presented analysis. In addition, the optimization algorithm determined whether the generator sets operated at continuous mode or periodical charge/discharge mode. In order to evaluate the actual fuel saving provided by the method when processing online, the algorithm was used in simulation of an Offshore Support Vessel (OSV) over seven operating modes. Although the online optimization had slightly less efficiency than the algorithm by around 1%, it provided an average fuel saving of around 15% compared to the conventional ac systems. The study also showed that the shipboard dc system with energy storage could provide a fuel saving of around 7% compared to the dc system without energy storage. The study results demonstrate significant fuel-saving potentials in maritime sector, particularly in the category of marine vessels that experience frequent load variations or long-time operation under non-rated conditions.

## Acknowledgments

This work has been supported by the Research Council of Norway and Det Norske Veritas (DNV) under project 179519, titled "Integrated Marine Electrical Power and Control Systems".

## Appendix

1) SFC characteristics:
   1.a. The support points for the specific fuel consumption of a 300 kW diesel engine: Table A.1
   1.b. The quadratic function coefficients of fuel consumption in terms of electrical power: Table A.2
2) The parameters of the generation units:
   2.a. Diesel engine: 6 cylinders, 30 rps, $K_y = 1.5e6$, 300 kW.
   2.b. The synchronous generator: 300 kVA, 320/460 V, 2 pole pairs, $J = 3.35$ kg.m$^2$, $r_s = 16.6$ mΩ, $r_{fd} = 5.245$ mΩ, $L_{lfd} = 0.68$ mH, $L_{ls} = 16.8$ mH, $L_{md} = 5.85$ mH, $L_{mq} = 5.05$ mH, $r'_{kd1} = 0.1526$ Ω, $L'_{lkd1} = 3.404$ mH, $L'_{lkq1} = 3.404$ mH, $r'_{kq1} = 40.57$ mΩ, $c_{Fe} = 3.4e\text{-}6$, $c_m = 0.15$.
   2.c. The rectifier: $V_{fw} = 1.5$ V, $R_{D,on} = 1.2$ mΩ.
   2.d. The PI controller of the governor: $K_P = 0.0077$, $K_I = 0.0165$.
   2.e. Voltage regulator–exciter: $K_P = 0.4$, $K_I = 0.2$, $T_{fb} = 0.01$ s, $T_{ff} = 1$ ms.
3) The parameters of the energy storage system:
   3.a. The low-voltage side of the dc/dc converter: $V_{LV} = 100$ V, $L = 516$ μH, $C_1 = 500$ μF, $n = 3$, $r_L = 3$ mΩ, $r_{C1} = 5$ mΩ,

$r_T = 3$ mΩ, $R_{S,on} = 0.6$ mΩ, $C_O = 50$ nF, $V_{fw} = 1.2$ V, $R_{D,on} = 1.2$ mΩ.

3.b. The high-voltage side of the dc/dc converter: $V_{HV} = 600$ V, $C_2 = 267$ μF, $r_{C2} = 0.34$ Ω, $R_{S,on} = 2.9$ mΩ, $C_O = 2.3$ nF, $V_{fw} = 0.8$ V, $R_{D,on} = 0.05$ mΩ.

3.c. Li-Ion battery parameters: $V_{full} = 93.1$ V, $V_{nom} = 80$ V, 1 kAh, $R_b = 0.8$ mΩ.

3.d. The ESS loss model parameters: $R_{bid} = 205$ mΩ, $R_{ess} = 0.3$ Ω, $P_{l0} = 100$ W.

4) Loss analysis for the boost mode:

$$p_{Sw,on} = \begin{cases} (2R_{S,on} \| 2R_{S,on}) i_L^2, & (0 \le t \le DT) \\ 2R_{S,on} i_L^2, & (DT \le t \le T) \end{cases} \tag{A.1}$$

$$P_{Sw,on} = R_{S,on} I_L^2 D + 2R_{S,on} I_L^2 (1-D) = (2-D) R_{S,on} I_L^2. \tag{A.2}$$

$$P_{Sw,sw} = 4\left(\frac{f_{sw}}{2}\right) C_O V_{SM}^2 = \frac{1}{2} f_{sw} C_O \frac{V_{hv}^2}{n^2}. \tag{A.3}$$

$$\begin{aligned} P_D &= 2V_{fw} I_{hv} + 2R_{D,on} I_{hv,rms}^2 \\ &= 2V_{fw} \frac{P_{hv}}{V_{hv}} + 2R_{D,on} \left(\frac{P_{hv}}{V_{hv}\sqrt{1-D}}\right)^2. \end{aligned} \tag{A.4}$$

$$P_L = r_L I_{L,rms}^2 = r_L \left(\frac{nP_{hv}}{(1-D)V_{hv}}\right)^2. \tag{A.5}$$

$$P_{C1} = r_{C1} I_{C1,rms}^2 = r_{C1} \left(\frac{DP_{hv}}{(1-D)V_{hv}}\right)^2. \tag{A.6}$$

$$P_{C2} = r_{C2} I_{C2,rms}^2 = r_{C2} \left(\frac{DV_{lv}}{\sqrt{12} f_{sw} L}\right)^2. \tag{A.7}$$

$$P_T = r_T I_{T,rms}^2 = r_T \left(\frac{nP_{hv}}{V_{hv}\sqrt{1-D}}\right)^2. \tag{A.8}$$

5) Analytical derivation of the fuel consumption:

5. a The energy balance of the dc bus over a charge–discharge cycle yields

$$\int_{T_c} P_{bus}(t)dt = \int_{T_{ch}} P_{bus}(t)dt + \int_{T_{dis}} P_{bus}(t)dt = 0. \tag{A.9}$$

where

$$P_{bus}(t) = \begin{cases} P_{s,k+1}(t) - P_L(t) - P_{l,ess}^{ch}(t) & 0 \le t < D_s T_c \\ P_{s,k}(t) - P_L(t) - P_{l,ess}^{dis}(t) & D_s T_c \le t < T_c \end{cases} \tag{A.10}$$

Replacing (A.10) in (A.9), we will have

$$\begin{aligned} &\int_{T_{ch}} [P_{s,k+1}(t) - P_L(t)]dt - \int_{T_{ch}} P_{l,ess}^{ch}(t)dt \\ &\quad + \int_{T_{dis}} [P_{s,k}(t) - P_L(t)]dt - \int_{T_{dis}} P_{l,ess}^{dis}(t)dt = 0. \end{aligned} \tag{A.11}$$

$$\begin{aligned} \int_{T_{ch}} P_{s,k+1}(t)dt + \int_{T_{dis}} P_{s,k}(t)dt &= \int_{T_{ch}} P_L(t)dt + \int_{T_{dis}} P_L(t)dt \\ &+ \int_{T_{ch}} P_{l,ess}^{ch}(t)dt + \int_{T_{dis}} P_{l,ess}^{dis}(t)dt. \end{aligned} \tag{A.12}$$

where the losses of the energy storage system are obtained by using (16) which yields

$$\begin{cases} P_{l,ess}^{ch}(t) = \frac{R_{ess}}{V_{bus}^2} (P_{s,k+1}(t) - P_L(t))^2. \\ P_{l,ess}^{dis}(t) = \frac{R_{ess}}{V_{bus}^2} (P_{s,k}(t) - P_L(t))^2. \end{cases} \tag{A.13}$$

The constant term of the ESS losses in (16) constitutes a power loss of 100 W. This constant value is considered as an additional load to the system loading so that only the second-order term will be included in the fuel consumption analysis.

In order to obtain (23) from (21) the following relations have been used. Similar relations hold for $P_{s,k}$.

$$\int_{T_{ch}} P_{s,k+1}^2(t)dt = P_{sa,k+1}^2 + \int_{T_{ch}} (P_{s,k+1}(t) - P_{sa,k+1})^2 dt. \tag{A.14}$$

$$\begin{aligned} \int_{T_{ch}} (P_{s,k+1}(t) - P_{sa,k+1})^2 dt &= \int_{T_{ch}} \alpha_{k+1}^2 (P_L(t) - P_{La})^2 dt \\ &= \alpha_{k+1}^2 T_{ch} R_{eq}^2. \end{aligned} \tag{A.15}$$

$$\begin{aligned} &\int_{T_{ch}} (P_{s,k+1}(t) - P_{sa,k+1})(P_L(t) - P_{La})dt \\ &= \int_{T_{ch}} \alpha_{k+1} (P_L(t) - P_{La})^2 dt = \alpha_{k+1} T_{ch} R_{eq}^2. \end{aligned} \tag{A.16}$$

$$\begin{aligned} a_{k+1} \int_{T_{ch}} P_{s,k+1}(t)dt + a_k \int_{T_{dis}} P_{s,k}(t)dt &= aP_{La}(T_{ch} + T_{dis}) \\ &+ aT_{ch} \frac{R_{ess}}{V_{bus}^2} \Big[ (P_{sa,k+1} - P_{La})^2 \\ &+ R_{eq}^2 \left(1 - 2\alpha_{k+1} + \alpha_{k+1}^2\right) \Big] \\ &+ aT_{dis} \frac{R_{ess}}{V_{bus}^2} \Big[ (P_{sa,k} - P_{La})^2 \\ &+ R_{eq}^2 \left(1 - 2\alpha_k + \alpha_k^2\right) \Big]. \end{aligned} \tag{A.17}$$

5. b The energy balance of the ESS over a charge–discharge cycle is used to find (25) by using the following relations.

$$\Delta E_{ch} + \Delta E_{dis} = 0. \tag{A.18}$$

$$\begin{aligned}\Delta E_{ch} &= \int_{T_{ch}} [P_{s,k+1}(t) - P_L(t)]dt - \int_{T_{ch}} P^{ch}_{l,ess}(t)dt \\ &= T_{ch}\left\{P_{sa,k+1} - P_{La} - \frac{R_{ess}}{V^2_{bus}}\left[(P_{sa,k+1} - P_{La})^2 + R^2_{eq}(1-\alpha_{k+1})^2\right]\right\}.\end{aligned} \tag{A.19}$$

$$\begin{aligned}\Delta E_{dis} &= \int_{T_{dis}} [P_{s,k}(t) - P_L(t)]dt - \int_{T_{dis}} P^{dis}_{l,ess}(t)dt \\ &= T_{dis}\left\{P_{sa,k} - P_{La} - \frac{R_{ess}}{V^2_{bus}}\left[(P_{sa,k} - P_{La})^2 + R^2_{eq}(1-\alpha_k)^2\right]\right\}.\end{aligned} \tag{A.20}$$

**Table A.1**
Specific fuel consumption against mechanical power.

| SFC (gr/kWh) | 85 kW | 150 kW | 220 kW | 300 kW |
|---|---|---|---|---|
| Fixed speed | 242 | 224 | 204.3 | 206 |
| Variable speed | 219 | 206.4 | 197 | 206 |

**Table A.2**
Quadratic function coefficients of fuel consumption against electrical power.

| Coefficients | $C_0$ (gr/h) | $a$ (gr/kWh) | $b$ (gr/kWh kW$^{-1}$) |
|---|---|---|---|
| Fixed speed | 12761.7 | 92.38 | 0.235 |
| Variable speed | 8488.1 | 115.65 | 0.202 |

## References


[1] A. Ådnanes, Maritime Electrical Installations and Diesel Electric Propulsion, ABB AS Marine, Oslo, 2003.
[2] J. Apsley, A. Gonzalez-Villasenor, M. Barnes, A. Smith, S. Williamson, J. Schuddebeurs, P. Norman, C. Booth, G. Burt, J. McDonald, IEEE Trans. Ind. Appl. 45 (2009) 676–684.
[3] P. Mitra, G. Venayagamoorthy, IEEE Trans. Power Electron. 25 (2010) 95–104.
[4] M. Bash, R.R. Chan, J. Crider, C. Harianto, J. Lian, J. Neely, S.D. Pekarek, S.D. Sudhoff, N. Vaks, in: IEEE Electric Ship Technologies Symposium, IEEE, 2009, pp. 560–567.
[5] R. Nilsen, I. Sorfonn, in: 13th European Conference on Power Electronics and Applications, 2009.
[6] B. Zahedi, L.E. Norum, IEEE Trans. Power Electron. 28 (2013) 4525–4537.
[7] J. Hansen, J. Lindtjørn, K. Vanska, in: Dynamic Positioning Conference, Marine Technology Society, 2011.
[8] J.F. Hansen, J.O. Lindtjorn, U.U. Odegaard, T.A. Myklebust, in: 4th International Conference on Technology and Operation of Offshore Support Vessels, 2011.
[9] M.C. Trummel, A.F. Burke, IEEE Trans. Veh. Technol. 32 (1983) 7–14.
[10] S. Barsali, M. Ceraolo, A. Possenti, IEEE Trans. Energy Convers. 17 (2002) 260–266.
[11] S. Williamson, M. Lukic, A. Emadi, IEEE Trans. Power Electron. 21 (2006) 730–740.
[12] A. Payman, S. Pierfederici, F. Meibody-Tabar, IEEE Trans. Power Electron. 24 (2009) 2681–2691.
[13] C.C. Chan, a. Bouscayrol, K. Chen, IEEE Trans. Veh. Technol. 59 (2010) 589–598.
[14] J. Popović-Gerber, J.A. Oliver, N. Cordero, T. Harder, J.A. Cobos, M. Hayes, S.C. O'Mathuna, E. Prem, IEEE Trans. Power Electron. 27 (2012) 2338–2353.
[15] P. Denholm, M. Kuss, R.M. Margolis, J. Power Sources 236 (2013) 350–356.
[16] R.T. Doucette, M.D. McCulloch, J. Power Sources 196 (2011) 1163–1170.
[17] K.H. Jansen, T.M. Brown, G.S. Samuelsen, J. Power Sources 195 (2010) 5409–5416.
[18] J. Neubauer, A. Brooker, E. Wood, J. Power Sources 236 (2013) 357–364.
[19] M. Shams-Zahraei, A.Z. Kouzani, S. Kutter, B. Bäker, J. Power Sources 216 (2012) 237–248.
[20] S.D. Breucker, E. Peeters, J. Driesen, in: IEEE Electric Ship Technologies Symposium, 2009, pp. 310–317.
[21] I.-Y. Chung, W. Liu, M. Andrus, K. Schoder, D.a. Cartes, M. Steurer, in: IEEE Electric Ship Technologies Symposium, IEEE, 2009, pp. 318–325.
[22] F. Dupriez-Robin, L. Loron, F. Claveau, P. Chevrel, in: IEEE Electric Ship Technologies Symposium, IEEE, 2009, pp. 270–277.
[23] O.C. Nebb, B. Zahedi, J.O. Lindtjorn, L.E. Norum, in: Vehicle Power and Propulsion Conference, IEEE, 2012, pp. 564–568.
[24] B.J. Vartdal, C. Chryssakis, in: International Scientific Conference on Hybrid and Electric Vehicles, 2011, pp. 1–12.
[25] Z. Jiang, J. Power Sources 177 (2008) 231–238.
[26] N. Khare, P. Singh, J. Power Sources 198 (2012) 368–377.
[27] G. Seenumani, H. Peng, J. Sun, J. Power Sources 196 (2011) 1599–1607.
[28] L.K.C. Tse, S. Wilkins, N. McGlashan, B. Urban, R. Martinez-Botas, J. Power Sources 196 (2011) 3149–3162.
[29] in: Maritime by Holland, Navigo, 2012, pp. 40–45.
[30] R.J. Wai, S.J. Jhung, J.J. Liaw, Y.R. Chang, IEEE Trans. Power Electron. 28 (2013) 3231–3244.
[31] O. Laldin, M. Moshirvaziri, O. Trescases, IEEE Trans. Power Electron. 28 (2013) 3882–3895.
[32] S. Lu, S. Hillmansen, C. Roberts, IEEE Trans. Veh. Technol. 60 (2011) 406–420.
[33] Y.L. Murphey, J. Park, Z. Chen, M.L. Kuang, M.A. Masrur, A.M. Phillips, IEEE Trans. Veh. Technol. 61 (2012) 3519–3530.
[34] S. Barsali, C. Miulli, A. Possenti, IEEE Trans. Energy Convers. 19 (2004) 187–195.
[35] C. Mademlis, J. Xypteras, N. Margaris, IEEE Trans. Power Electron. 13 (1998) 288–296.
[36] J. Lai, D. Nelson, Proc. IEEE 95 (2007) 766–777.
[37] M. Yilmaz, P.T. Krein, IEEE Trans. Power Electron. 28 (2013) 2151–2169.
[38] M.K. Kazimierczuk, Pulse-width Modulated DC–DC Power Converters, first ed., Wiley, 2008.
[39] A.P. Schmidt, M. Bitzer, A.W. Imre, L. Guzzella, J. Power Sources 195 (2010) 5071–5080.
[40] V.R. Subramanian, V. Boovaragavan, V. Ramadesigan, M. Arabandi, J. Electrochem. Soc. 156 (2009) A260–A271.
[41] C.Y. Wang, V. Srinivasan, J. Power Sources 110 (2002) 364–376.
[42] X. Hu, S. Li, H. Peng, J. Power Sources 198 (2012) 359–367.
[43] O. Tremblay, L.A. Dessaint, A.I. Dekkiche, in: Vehicle Power and Propulsion Conference, 2007. VPPC 2007, IEEE, 2007, pp. 284–289.